

Propagation and Structure of Edge Diffusion Flames in Axisymmetric Hydrocarbon Fuel Jets

Fumiaki Takahashi*

National Center for Microgravity Research on Fluids and Combustion
NASA Glenn Research Center, Cleveland, Ohio 44135

Viswanath R. Katta

Innovative Scientific Solutions, Inc., Dayton, Ohio 45440

Keywords: edge diffusion flames, flame propagation, flame structure, flame stabilization

Abstract

The transient behavior and internal structure of a flame propagating through a flammable layer, formed in a fixed mixing time after issuing an axisymmetric fuel jet into air, have been simulated numerically in normal- or zero gravity. A detailed chemical reaction mechanism was used for C₁-C₃ hydrocarbon fuels, including methane, ethane, ethylene, acetylene, and propane. The calculated flame edge displacement velocity almost reached the laminar flame speed of the stoichiometric fuel-air mixture for each fuel independent of gravity. The vigorously burning reaction kernel in the leading flame possessed characteristics of premixed flames in the direction of propagation with unique flame structure in the transverse direction and piloted a trailing diffusion flame.

INTRODUCTION

Diffusion flame stabilization is of essential importance in both Earth-bound combustion systems and spacecraft fire safety. Local extinction and re-ignition processes can occur in both cases as a result of interactions between the flame zone and vortices or fire-extinguishing agents. The issue of secondary fires where fires jump from one location to another is also an important issue in fire safety. In such circumstances, the dynamic behavior of edge diffusion flames may play a key role in a fate of fires.

In previous papers [1-4], by using a comprehensive computational fluid dynamics code [5] with a detailed chemistry model for methane combustion, the authors have revealed the complex chemical kinetic structure of the stabilizing region of both jet and flat-plate diffusion flames, predicted the flame stability limit, and proposed diffusion flame attachment and detachment mechanisms. Because of the unique geometry of the edge of diffusion flames, radical back-diffusion against the oxygen-rich entrainment flow dramatically enhances chain-branching and exothermic reactions, thus forming a peak reactivity spot, i.e., *reaction kernel*, which is responsible for flame stabilization.

In the previous experiment and computation, a cold fuel jet was ignited around the centerline downstream, and the flame quickly propagated along the mixing layer toward the burner rim. This transient flame propagation provides a unique configuration suitable to study the structure of an unstationary flame through a stratified mixing layer. This paper reports new results for the initial flame propagation and structure using up to C₃ hydrocarbons.

COMPUTATIONAL METHOD

The numerical code (UNICORN) developed by Katta et al. [5], described in more detail elsewhere [2], was used in this study. Time-dependent two-dimensional governing equations consist of continuity, full Navier-Stokes momentum, energy, and species conservation equations with the ideal-gas equation of state. A body-force term caused by the gravitational field is included in the axial momentum equation. The momentum equations are integrated using an implicit QUICKEST numerical scheme for the convection terms, which is third-order accurate in both space and time and has a very low numerical-diffusion error. The finite-difference form of the species and enthalpy is obtained using the hybrid scheme with upwind and central differences. The coefficients of viscosity, thermal conductivity, and diffusion are estimated using molecular dynamics and mixture rules. The enthalpy of each species is calculated from polynomial curve-fits. The detailed C₃-chemistry model [6, 7] (33 species and 112 elementary steps) used includes the identical C₁- and C₂-chemistry portions previously used [1-4]. A simple radiation model [8] based on an optically thin-media assumption was incorporated into the energy equation for radiative heat losses from CO₂, H₂O, CH₄, and CO.

The computational domain of 60 × 50 mm in the axial (*z*) × radial (*r*) directions is represented by a mesh of up to 601 × 201 with clustered grid lines near the jet exit with a minimum spacing of 0.05 mm. The inner diameter and lip thickness of the fuel tube are *d* = 3 mm and 0.5 mm, respectively. The fuel tube exit plane is placed 10 mm

* Corresponding author: Fumiaki.Takahashi@grc.nasa.gov

downstream from the inflow boundary in the open computational domain. Fully developed pipe flow in the fuel tube and boundary layer velocity profiles outside the burner tube are used. The initial and boundary conditions for the axial (U) and radial (V) velocities and species and energy at different flow boundaries are the same as in previous work [1-4]. Table 1 shows the test conditions. The fuel jet velocity of each fuel is proportional to the stoichiometric fuel requirement per unit volume of oxygen. The ambient air velocity is negligibly small ($U_a = 0.001$ m/s) for all cases.

TABLE 1 Test conditions

Case	Fuel	U_i (m/s)	Gravity
1	Methane	0.1200	0g
2	Ethane	0.0686	0g
3	Ethylene	0.0800	0g
4	Acetylene	0.0960	0g
5	Propane	0.0480	0g
6	Ethane	0.0686	1g

RESULTS AND DISCUSSION

Figure 1 shows the temporal sequences of the

calculated temperature fields in ethane flames in 0g and 1g. In each case, the cold fuel jet issued for 0.3 s prior to ignition. Then the fuel jet was ignited by raising the temperature and radical concentrations for a short period (0.2 ms) in a small region (0.05 mm length \times 0.9 mm radius) at the centerline location where the stoichiometric mixture was formed. The edge of the flame propagated through the fuel-air mixing layer formed almost spherically. In both cases of 0g and 1g, the flame reached the burner at the same time ($t = 22$ ms, Figs. 1d and 1j). After the flame attachment, the thermal layer continued to diffuse outwardly in 0g (Fig. 1f), and the buoyancy-induced flow blew the hot gases upward in 1g (Fig. 1l),

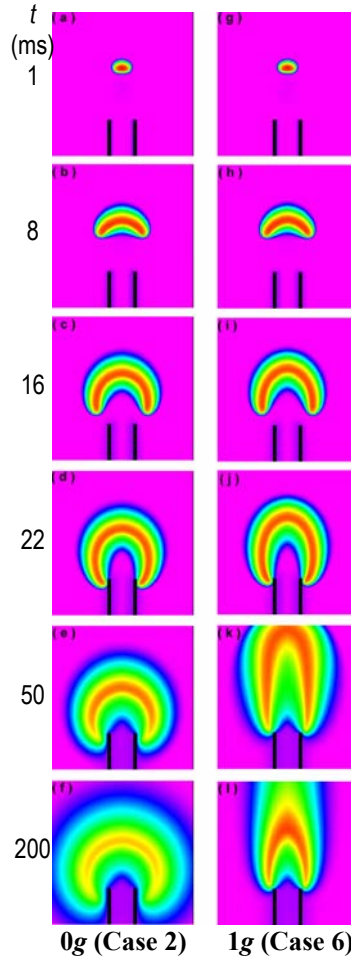


Fig.1 Calculated temperature field in an ethane flame in air.

approaching to a steady flame.

The leading flame displacement velocity vector (\mathbf{v}_f) and its angle (θ_f) with respect to the horizon were determined from the animated temperature field images. Because the flow velocity ahead of the flame is negligibly small (<2 mm/s), the displacement velocity can be approximated as the flame propagation velocity relative to the fluid. Figures 2 and 3 show the displacement velocity and angle for all fuels in 0g. Table 2 summarizes the average displacement velocities ($|\bar{v}_f|$) and the stoichiometric laminar flame speed (S_L) data in the literature [9].

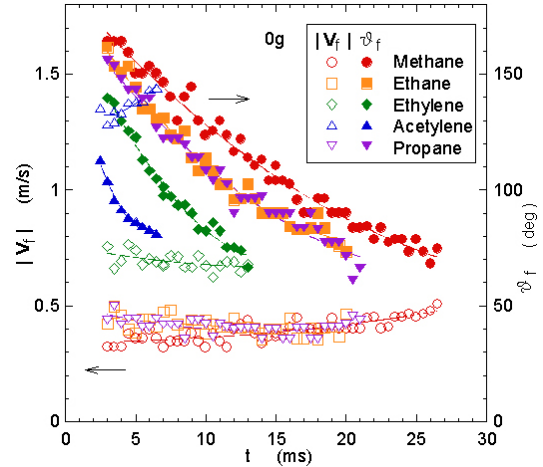


Fig. 2 Calculated flame displacement velocity and angle for various fuels in air in 0g (Cases 1-5).

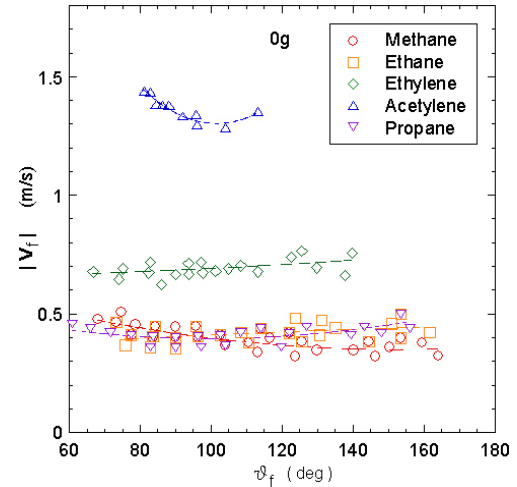


Fig. 3 Calculated flame-base displacement velocity vs. angle for various fuels in air in 0g (Cases 1-5).

TABLE 2 Average flame displacement velocity

Fuel	$ \bar{v}_f $ (cm/s)	S_L at $\phi=1$ (cm/s)
Methane	39.3 (0g)	43.4
Ethane	41.4 (0g)/40.7 (1g)	44.5
Ethylene	69.1 (0g)	68.0
Acetylene	136.2 (0g)	144
Propane	41.0 (0g)	45.6

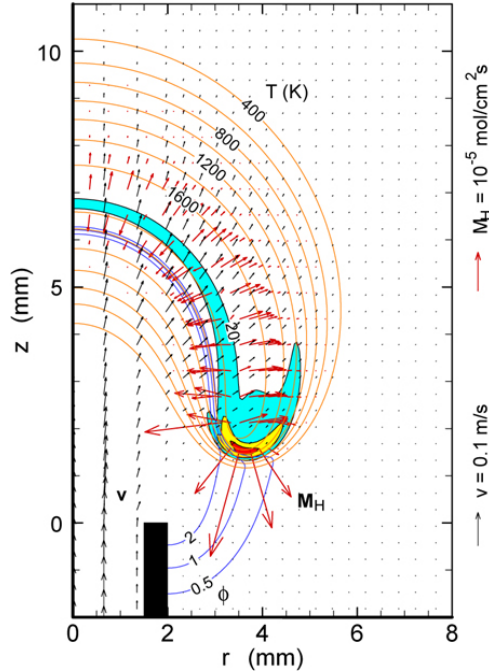


Fig. 4 Velocity vectors, isotherms, heat-release rate (20, 100, and 300 J/cm³s), equivalence ratio, and total molar flux vectors of hydrogen atoms in an ethane flame in 0g (Case 2). $t = 16$ ms.

There is an excellent correlation between these quantities as $|\bar{v}_f| = 0.9475S_L$ with $R = 0.99797$. This result is important because the computations were conducted using a multi-species multi-step chemical reaction mechanism for various fuels without adjustable kinetic parameters and the reaction kernel possessed the structure capable to consume the reactants at rates as close to those for stoichiometric premixed flames.

Figure 4 shows the calculated structure of an ethane flame in 0g at the elapse time of 16 ms (cf. Fig. 1c), including the velocity vectors (\mathbf{v}), isotherms (T), total heat-release rate (\dot{q}), equivalence ratio (ϕ), and molar flux vectors of atomic hydrogen (\mathbf{M}_H). The heat-release rate shows a peak reactivity spot (i.e., the reaction kernel) at the flame base. The heat-release rate reached a sharp peak of 378 J/cm³s. The oxygen consumption rate (not shown) shows a sharp peak (0.001198 mol/cm³s) at the same location with the heat-release rate peak. The velocity, temperature, and the equivalence ratio at the reaction kernel were 0.0065 m/s, 1436 K, and 0.49, respectively. The saddle-shaped high reactivity area faced toward the direction of the flammable mixture zone approximated with the layer between $\phi = 0.5$ and 2 curves shown. The isotherms show particularly narrow intervals below the reaction kernel in the direction of the flame propagation. The velocity vectors show acceleration and outward deflection in the high temperature region as a result of thermal gas expansion. The hydrogen atom (and the OH radical and the O atom, not shown) diffused onto both sides of the trailing diffusion flame zone

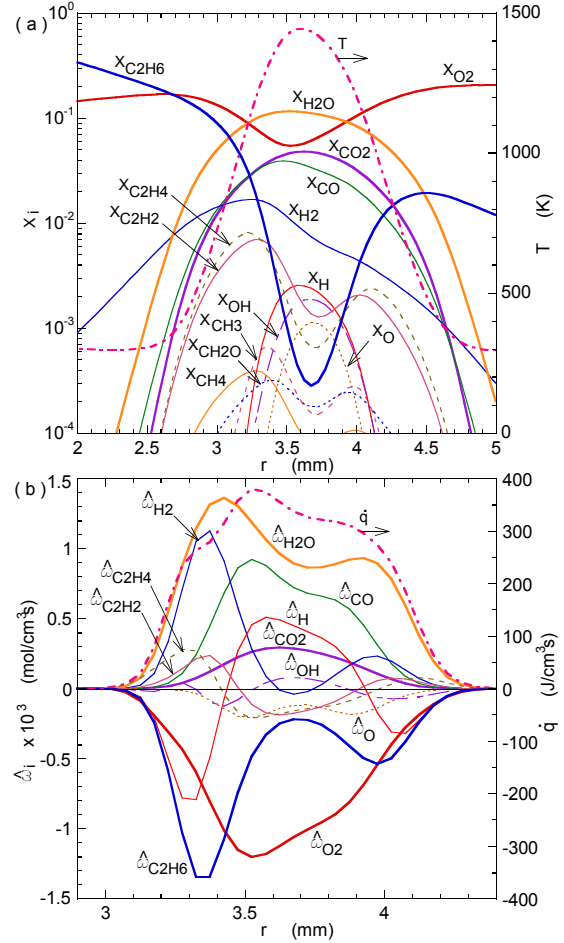


Fig. 5 Calculated reaction kernel structure (horizontal) in an ethane flame in 0g (Case 2). $t = 16$ ms. $z = 1.58$ mm. (a) Mole fractions, temperature, (b) species formation rates, and heat-release rate.

and every downward directions into the high oxygen concentration region below the reaction kernel.

Figure 5 shows the horizontal variations of the species mole fractions (X_i), temperature, species formation rate ($\hat{\omega}_i$), and heat-release rate across the reaction kernel. The overall structure resembled to that of the 1g stationary methane flame with the standoff distance of several mm [2], except for the air side of the flame, where leftover fuel remained at relatively high concentrations, forming unique flame structure somewhat mirrored to the fuel side with smaller peaks of the species formation rates. On the fuel side and, to some extent, the air side, there the fuel (ethane) was destroyed by the H atom attack and ethylene, acetylene, and molecular hydrogen were formed. Major differences between the present propagating flame and the stationary flames previously studied stem from the mixing time and the fuel type. The reaction zone in the propagating flame broadened radially as a result of the thicker flammable mixture layer (~1.2 mm) compared to the stationary flame (0.6-0.8 mm [2, 3]). There was 0.3 s of the fuel-air mixing

time prior to ignition in a still environment, whereas in the stationary flames, the mixing occurred within a residence time (~ 0.01 s order) of the fluid particles over the standoff distance (4-9 mm) in a coflowing air (~ 0.7 m/s). Secondly, in the present case, the C_2 -route in the oxidation process dominated over the C_1 route. The contributions to the total heat-release rate by the C_2 exothermic reactions, $\text{CHCO} + \text{O} \rightarrow \text{CO} + \text{CO} + \text{H}$ (R59) and $\text{C}_2\text{H}_2 + \text{O} \rightarrow \text{CH}_2 + \text{CO}$ (R60) exceeded the C_1 reaction, $\text{CH}_3 + \text{O} \rightarrow \text{CH}_2\text{O} + \text{H}$ (R46).

Figure 6 shows the axial variations of the variables through the reaction kernel nearly coincident with the direction of flame propagation. The flame structure shows characteristics of premixed flames: high concentrations of fuel and oxygen (nearly at a stoichiometric proportion) in the approaching fuel-air mixture decreased toward the flame zone, while those of combustion products increased and the temperature increased. More precisely, a chain of events occur in the direction opposite to the flame propagation. The chain radicals, formed in the high temperature zone, diffused back toward the preheat zone, the H attack on O_2 molecules formed HO_2 at relatively low temperatures, ethane was dehydrogenated by the radical attack to ethylene and then acetylene, forming H_2 and H_2O , and the fuel carbon was oxidized to CO and then CO_2 . The reaction zone thickness was approximately 0.5 mm.

CONCLUSIONS

The numerical simulations of C_1 to C_3 hydrocarbon flames using a detailed chemical reaction mechanism have revealed the propagation behavior and the internal structure of the reaction kernel of unstationary edge diffusion flames in both 1g and 0g environments. The calculated leading flame edge displacement velocity through the flammable mixture layer in cold fuel jets nearly reached the laminar flame speed of the stoichiometric fuel-air mixture for each fuel. The reaction kernel, which broadened radially facing the direction toward the flammable mixture layer, possessed characteristics typical of premixed flames in the direction of the flame propagation with unique features in the transverse direction and led a trailing diffusion flame.

ACKNOWLEDGMENT

This work was supported in part by the NASA Office of Biological and Physical Research, Washington, DC, and in part by the U.S. Air Force Office of Scientific Research.

REFERENCES

1. Takahashi, F. and Katta, V. R., *Proc. Combust. Inst.* 27:675 (1998).
2. Takahashi, F. and Katta, V. R., *Combust. Sci. Technol.* 155:243 (2000).
3. Takahashi, F. and Katta, V. R., *Proc. Combust. Inst.* 28:2071 (2000).
4. Takahashi, F. and Katta, V. R., *Proc. Combust. Inst.* 29:

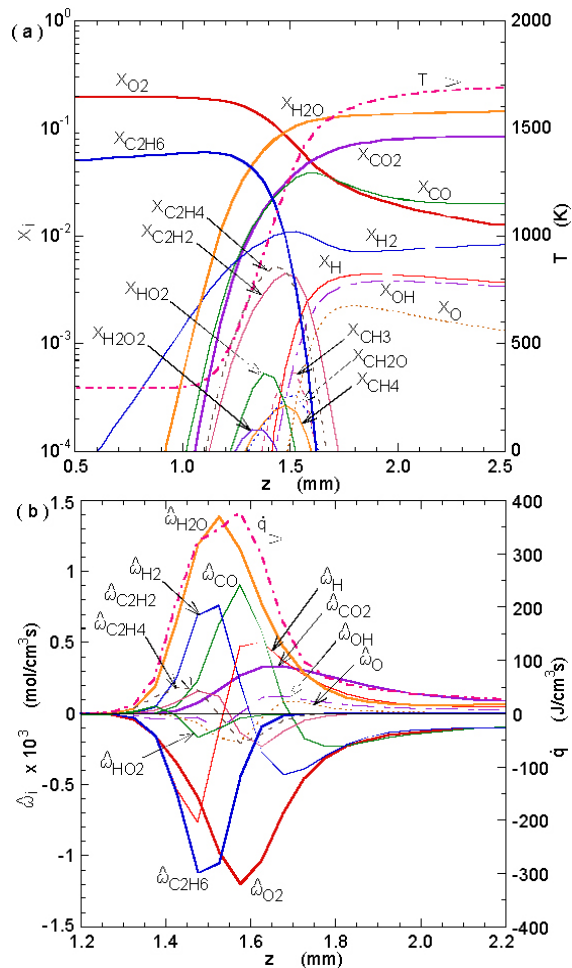


Fig. 6 Calculated reaction kernel structure (vertical) in an ethane flame in 0g (Case 2). $t = 16$ ms. $r = 3.54$ mm. (a) Mole fractions, temperature, (b) species formation rates, and heat-release rate.

in press (2002).

5. Katta, V. R., Goss, L. P., and Roquemore, W. M., *AIAA J.* 32:84 (1994).
6. Peters, N., in *Reduced Kinetic Mechanisms for Applications in Combustion Systems* (N. Peters and B. Rogg, Eds.), Springer-Verlag, Berlin, 1993, pp. 3-14.
7. Warnatz, J., in *Combustion Chemistry* (W. C. Gardiner, Ed.), Springer-Verlag, New York, 1984, p. 197-360.
8. Annon., Radiation Models, International Workshop on Measurement and Computation of Turbulent Nonpremixed Flames, <http://www.ca.sandia.gov/TNF/radiation.html>, 2003.
9. Glassman, I., *Combustion*, 3rd ed., Academic Press, San Diego, 1996.